

SWIFT/BAT DETECTION OF HARD X-RAYS FROM TYCHO'S SUPERNOVA REMNANT: EVIDENCE FOR TITANIUM-44

E. TROJA^{1,2}, A. SEGRETO³, V. LA PAROLA³, D. HARTMANN⁴, W. BAUMGARTNER¹, C. MARKWARDT¹, S. BARTHELMY¹, G. CUSUMANO³, AND N. GEHRELS¹

Draft version February 3, 2018

ABSTRACT

We report *Swift*/BAT survey observations of the Tycho's supernova remnant, performed over a period of 104 months since the mission's launch. The remnant is detected with high significance ($>10\sigma$) below 50 keV. We detect significant hard X-ray emission in the 60-85 keV band, above the continuum level predicted by a simple synchrotron model. The location of the observed excess is consistent with line emission from radioactive Titanium-44, so far reported only for Type II supernova explosions. We discuss the implications of these results in the context of the galactic supernova rate, and nucleosynthesis in Type Ia supernova.

Subject headings: gamma rays; observations; supernova remnants; nuclear reaction, nucleosynthesis, abundances

1. INTRODUCTION

Radioactive elements produced during a supernova (SN) explosion carry unique information about the explosive nucleosynthesis process, the stellar progenitor, and the explosion mechanism itself. An element of great astrophysical interest is Titanium-44, which, with a half-life of ~ 59 yr (Ahmad et al. 2006), can give rise to observable features in the spectra of young supernova remnants (SNRs). The $^{44}\text{Ti} \rightarrow ^{44}\text{Sc} \rightarrow ^{44}\text{Ca}$ decay chain produces three de-excitation lines of roughly equal branching ratios, at 1157 keV (from ^{44}Ca), and at 78.4 keV, and 67.9 keV (from ^{44}Sc). Observations of young SNRs in the gamma-ray and hard X-ray bands therefore represent a promising window into the latest stages of stellar evolution (Clayton et al. 1969; Leising 2001; Vink 2012).

The first direct evidence of ^{44}Ti was found by the *Compton Gamma Ray Observatory* (Iyudin et al. 1994) in the SNR Cassiopea A. The daughter ^{44}Sc emission lines were later detected in the hard X-ray band by *Beppo-SAX* (Vink et al. 2001), and *INTEGRAL* (Renaud et al. 2006a). The observed flux of $\approx 2 \times 10^{-5}$ photons $\text{cm}^{-2} \text{s}^{-1}$ in each line implies a ^{44}Ti mass of $\approx 2 \times 10^{-4} M_{\odot}$, consistent with a core-collapse origin (Krause et al. 2008a; Chieffi & Limongi 2013). The spatial distribution of the Scandium lines, as recently imaged by *NuSTAR* (Harrison et al. 2013), provides strong evidence for an asymmetric explosion, likely caused by low-mode convection (Grefenstette et al. 2014).

For SNe Type Ia, sub-Chandrasekhar mass models (Woosley & Weaver 1994) can synthesize large amounts of radioactive of ^{44}Ti , exceeding $10^{-3} M_{\odot}$ in some scenarios (Fink et al. 2010; Woosley & Kasen 2011). The ^{44}Ti yield is probably less abundant in normal Type Ia explosions, ranging from $\sim 10^{-6} M_{\odot}$ for a centrally-ignited pure-deflagration to $\lesssim 6 \times 10^{-5} M_{\odot}$ for an off-center de-

layed detonation (Iwamoto et al. 1999; Maeda et al. 2010). Indeed, previous attempts to detect radioactive lines in SN Ia remnants were unsuccessful (Dupraz et al. 1997; Renaud et al. 2006b). The historical Tycho remnant, originated in 1572AD from a Type Ia SN (Baade 1945; Krause et al. 2008b), has been a primary target for searching nuclear emission lines. A 1.5 Ms long observation by *INTEGRAL* detected the X-ray continuum only up to energies of ~ 50 keV, placing a 3σ upper limit of 1.5×10^{-5} photons $\text{cm}^{-2} \text{s}^{-1}$ on the flux of the ^{44}Sc lines (Renaud et al. 2006b; Wang & Li 2014).

In this Letter we report first evidence of significant emission above 50 keV from the Tycho SNR, detected by the Burst Alert Telescope (BAT; Barthelmy et al. 2005) on-board *Swift* (Gehrels et al. 2004). The signal is detected at a ~ 4 sigma confidence level in the 60-85 keV energy band, consistent with the location of the Scandium lines. Our observations and data analysis are described in Section 2. Our results are discussed in Section 3. Unless otherwise stated, the quoted uncertainties represent the 90% confidence interval for one interesting parameter, corresponding to $\Delta\chi^2=2.706$ (Lampton et al. 1976).

2. DATA ANALYSIS

2.1. Observations and Data Reduction

Since its launch in November 2004, *Swift* is performing an all-sky survey with the BAT, covering the 14-195 keV energy range. Thanks to the BAT's wide field of view (1.4 sr, half-coded), its large detector area (5432 cm^2), and the random *Swift* pointing strategy, the BAT Survey resulted in the most sensitive and uniform coverage of the hard X-ray sky (Tueller et al. 2010; Cusumano et al. 2010; Baumgartner et al. 2013).

We analyzed the data from November 2004 until July 2013, spanning a period of 104 months since the mission's launch. The BAT survey raw data were retrieved from the *Swift* public archive⁵ where they are stored in the form of detector plane histograms: three-dimensional arrays (two spatial dimensions, one spectral dimension)

¹ NASA, Goddard Space Flight Center, Greenbelt, MD

² Department of Physics and Astronomy, University of Maryland, College Park, MD

³ INAF - IASF Palermo, via Ugo La Malfa, Italy

⁴ Department of Physics and Astronomy, Clemson University, Clemson, SC

⁵ <http://heasarc.gsfc.nasa.gov/cgi-bin/W3Browse/swift.pl>

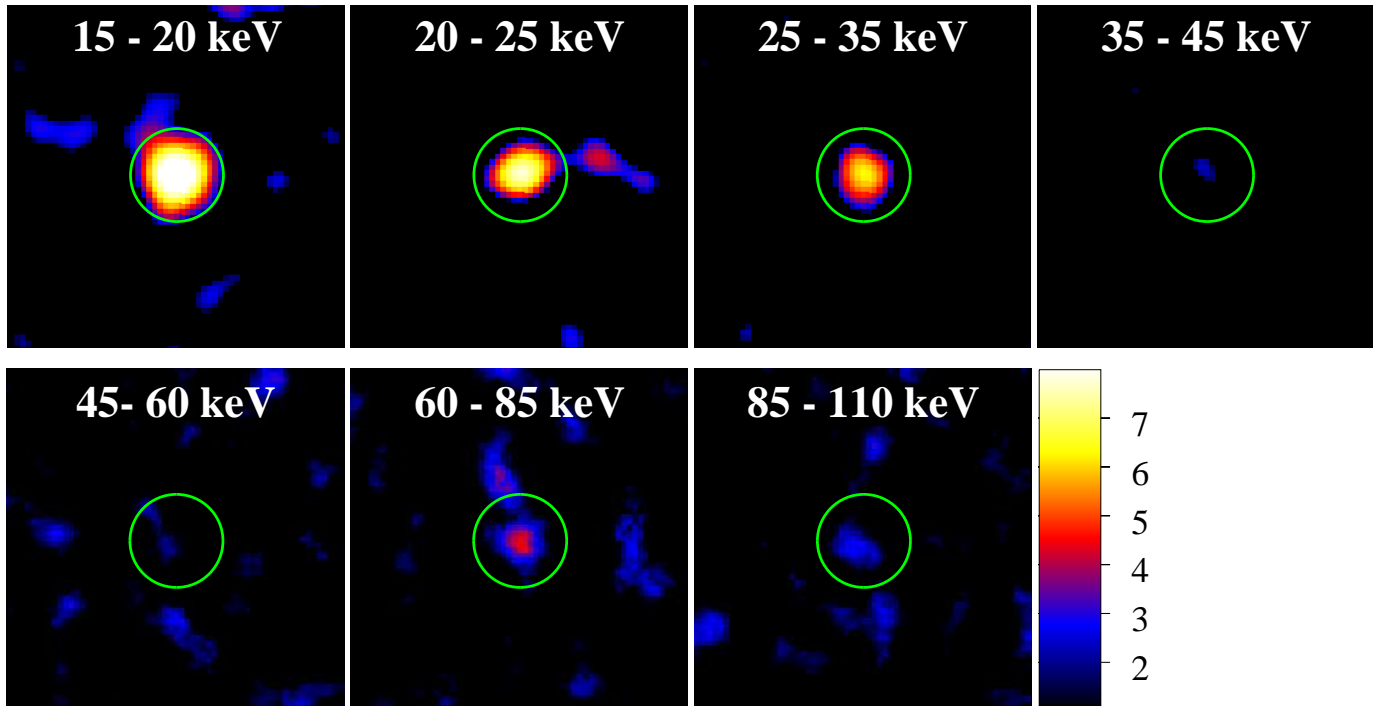


FIG. 1.— *Swift*/BAT image of Tycho’s SNR in different energy ranges. The SNR position is indicated by the green circle. The color scale is proportional to the detection significance in units of standard deviations.

that collect count-rate data in 5-min time bins for 80 energy channels. These data were processed with a dedicated software (Segreto et al. 2010) that computes all-sky maps in 8 energy bands between 15 and 150 keV, performs source detection on these maps, and for each detected source produces standard products such as background subtracted light curves and spectra.

The Tycho’s SNR is detected in the 15–150 keV all-sky map with a signal to noise ratio of 15.6 standard deviations. The source was inside the BAT field of view for approximately 43 Ms, corresponding to a total on-axis equivalent exposure of 19.6 Ms. An image of the SNR in different energy channels is presented in Figure 1. The source is detected with high significance in the low energy channels (<35 keV), and only marginally in the 35–45 keV energy range. The detection significance in the 60–85 keV bin has been growing with time, from 3.4σ (using the first 25 months of survey data), to 3.9σ (50 months), and to 4.7σ (75 months).

An independent analysis, based on the products of the standard GSFC pipeline (Tueller et al. 2010; Baumgartner et al. 2013), finds consistent results. The GSFC processing (Baumgartner et al. 2013) covers the period from November 2004 through August 2013, for a total on-axis exposure of 19.6 Ms. Data are rebinned into eight survey energy bands between 14 keV and 195 keV. The SNR is detected with high-significance below 35 keV, and with lower significance in the 50–75 keV (2.4σ), and 75–100 keV (3.5σ) energy bands.

As the detected signal above 50 keV is faint, background modeling and subtraction is of critical importance in its analysis. The analysis technique for BAT coded mask data inherently subtracts the background, as discussed in more detail in Segreto et al. (2010) and Baumgartner et al. (2013). Imperfections in subtraction

of non-imaged background are apparent as pattern noise in the resulting all-sky images from which the SNR flux values are derived. The significance of the flux properly accounts for pattern noise, in addition to Poisson noise.

2.2. Spectral analysis

The continuum shape is a critical element for determining the nature of the emission above 50 keV. The most likely origin of the hard X-ray continuum in the Tycho’s SNR is synchrotron radiation from a population of shock-accelerated electrons. Both *Suzaku* (Tamagawa et al. 2009) and *Chandra* (Hwang et al. 2002; Eriksen et al. 2011) observations are consistent with a simple power-law of photon index $\Gamma \approx 2.8$. However, the SNR’s broadband spectrum deviates from a simple power-law, showing a gradual turn-over at energies $E \approx 1$ keV. In this case, a simple power-law model might overestimate the contribution of the continuum above 60 keV. We therefore modelled the continuum shape by using a power-law function as well as a synchrotron cutoff model (model *srcut*; Reynolds & Keohane 1999) with low-energy slope $\alpha = 0.65$, and a 1.4 GHz flux density of 40.5 Jy (Kotthes et al. 2006).

Spectral fits were performed with XSPEC v.12.8.1 by minimizing the χ^2 statistics. All the fits were carried out in the 15–110 keV energy band. The power-law fit yields a photon index $\Gamma = 3.0 \pm 0.3$, consistent with previous *Chandra* and *Suzaku* results, and a $\chi^2 = 18$ for 5 degrees of freedom (d.o.f.). The *srcut* fit yields a $\chi^2 = 20$ for 6 d.o.f. and a break frequency $\nu_b = (2.00 \pm 0.12) \times 10^{17}$ Hz, in agreement with the values quoted by Tamagawa et al. (2009) and Eriksen et al. (2011). The poor fits are mainly due to the signal detected in the 60–85 keV bin, which lies 4σ above the predicted continuum decay. We mod-

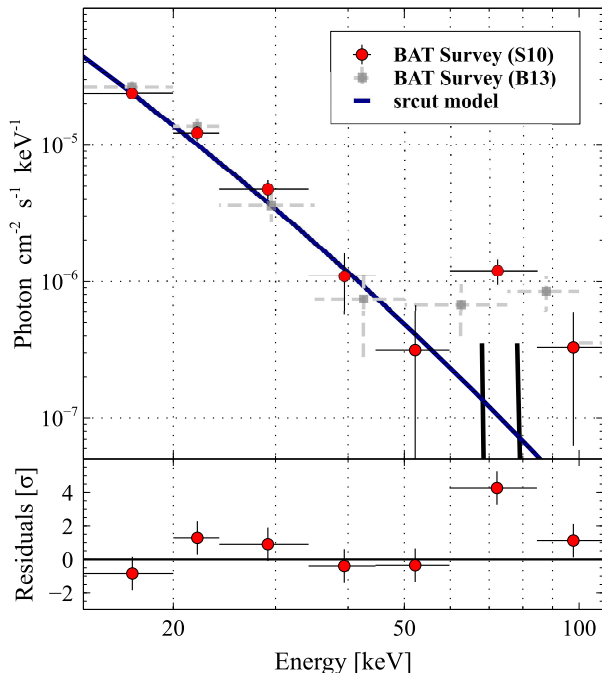


FIG. 2.— BAT spectrum of the Tycho's SNR. We show the survey data processed with the Segreto et al. (2010) pipeline (S10), used for the spectral analysis, and, for comparison, the survey data processed with the GSFC pipeline (B13). The best fit model for the hard X-ray continuum is a synchrotron model (srcut function), shown as a solid line. The two vertical lines mark the energies of the ^{44}Sc lines. The bottom panel shows the fit residuals in units of sigma.

elled the observed excess with two gaussian profiles at fixed centroids of 68 keV and 78 keV, zero width, and relative flux ratio $F_{68}=0.93 F_{78}$. The resulting fits are acceptable, with the srcut model ($\chi^2=6.2$ for 5 d.o.f.) being statistically preferred over the simple power-law ($\chi^2=7.4$ for 4 d.o.f.). The SNR spectrum and the best fit model (without the contribution of the ^{44}Sc lines) are reported in Figure 2. The derived fluxes for the two lines are $F_{78}=(1.4\pm 0.6)\times 10^{-5}$ photons $\text{cm}^{-2} \text{s}^{-1}$, and $F_{68}=(1.3\pm 0.6)\times 10^{-5}$ photons $\text{cm}^{-2} \text{s}^{-1}$. We further investigated the dependence of the lines flux on the underlying continuum shape. Figure 3 shows the confidence level contours of the 78 keV line flux as a function of the break frequency. The resulting 3σ error range is $2.1\times 10^{-6} < F_{78} < 2.6\times 10^{-5}$ photons $\text{cm}^{-2} \text{s}^{-1}$.

A different possibility is that the observed excess is due to an additional continuum component, such as non-thermal bremsstrahlung emission. We therefore added to our continuum model a power-law component. The resulting fit with a synchrotron+power-law model is poor ($\chi^2=12$ for 4 d.o.f.). In fact, the power-law flux in the 60-85 keV bin is constrained to $\lesssim 0.8\times 10^{-6}$ photons $\text{cm}^{-2} \text{s}^{-1}$ by the non-detections in the adjacent 45-60 keV, and 85-110 keV bins, and cannot account for all the observed emission.

In order to check whether the observed excess in the 65-80 keV band could be an artifact we performed the following tests: 1) after excluding the point sources, we checked that the statistical distribution of the skymap pixels significances is a gaussian distribution with mean 0 and standard deviation 1; 2) we checked that spectra extracted at random source-free positions did not present

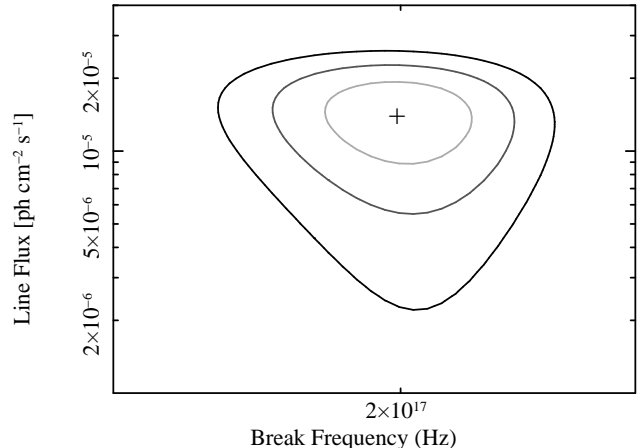


FIG. 3.— Confidence contours for the line flux F_{78} and the synchrotron frequency ν_b . The best fit value is marked by the cross symbol. The confidence levels are 1, 2, and 3σ for two parameters of interest, corresponding to $\Delta\chi^2=4.61, 6.17,$ and 11.8 (Lampton et al. 1976).

any feature, and were consistent with zero; 3) we checked that the detected sources located near the Tycho's SNR did not present the same 65-80 keV excess in their spectra, nor any other peculiar feature. In particular, this last point allows us to exclude that the observed feature is a systematic effect related to the response matrix.

2.2.1. Consistency check: the SNR Cas A

The same data reduction and analysis was applied to the BAT spectrum of the SNR Cas A, which is a known source of ^{44}Ti . The SNR was within the BAT FoV for 44 Ms, corresponding to an on-axis equivalent exposure of 19.9 Ms. The signal in the 60-85 keV range is detected with high significance ($>13\sigma$).

Also in this case, as expected, the fit with a simple power-law function is not acceptable ($\chi^2=68$ for 5 d.o.f.), as it significantly underestimates the flux in the 60-85 keV bin. We therefore modelled the spectrum with a power-law function for the continuum, and two narrow gaussian features at the position of the ^{44}Sc lines. This model provides a good description of the dataset ($\chi^2=5.4$ for 4 d.o.f.), with best fit values $\Gamma=3.32\pm 0.07$ for the power-law photon index, $A=(1.5\pm 0.3)\times 10^{-5}$ photons $\text{cm}^{-2} \text{s}^{-1}$ at 1 keV for the power-law normalization, $F_{78}=(2.7\pm 0.6)\times 10^{-5}$ photons $\text{cm}^{-2} \text{s}^{-1}$, and $F_{68}=(2.5\pm 0.6)\times 10^{-5}$ photons $\text{cm}^{-2} \text{s}^{-1}$ for the fluxes of the two lines. The derived fluxes are in excellent agreement with previous measurements from BeppoSAX (Vink et al. 2001), and INTEGRAL (Renaud et al. 2006a), and slightly higher than the value measured by *NuSTAR* (Grefenstette et al. 2014). The observed X-ray emission from ^{44}Sc is indeed expected to decay with time. As our data span a period of ~ 9 years prior to the *NuSTAR* observations, the expected decrease in the line flux is $<10\%$, and can partially account for the observed difference. Another possibility is that a small fraction of the observed flux comes from a spatially diffuse component of emission, which was not imaged by *NuSTAR*.

3. RESULTS

The most notable feature of the BAT observations is the detection of emission in the 60–85 keV range. The SNR spectrum is well described by a simple synchrotron model, which also provides the best description of the broadband (from radio to hard X-rays) emission (e.g. Slane et al. 2014). However, this model fails to reproduce the observed signal above 60 keV. The BAT non-detection above 85 keV constrains the contribution of any additional continuum component to be negligible. This is in agreement with the SNR properties (low gas density, and high magnetic field) inferred by other studies, which also imply a weak non-thermal bremsstrahlung.

Although the broad spectral bins do not allow us to clearly resolve the two emission lines, the energy range of the observed excess is remarkably consistent with the location of the ^{44}Ti nuclear lines. By attributing the observed signal above 60 keV to the ^{44}Sc lines, we can estimate the ^{44}Ti yield as (e.g. Grebenev et al. 2012):

$$\frac{M(\text{Ti})}{M_{\odot}} = 1.41 \times 10^{-4} \left[f_X \left(\frac{d}{1 \text{ kpc}} \right)^2 \tau \exp \left(\frac{T}{\tau} \right) W^{-1} \right], \quad (1)$$

where f_X is the observed line flux in units of photons $\text{cm}^{-2} \text{s}^{-1}$, d the SNR distance, T its age, and $\tau = 85.3 \pm 0.4$ yr the ^{44}Ti lifetime (Ahmad et al. 2006). The emission efficiencies for the two lines are $W_{68} = 0.877$, and $W_{78} = 0.947$, respectively.

As shown in Equation 1, the estimated mass sensitively depends on the SNR distance. Various measurements constrain d in the range between 1.5 and 5 kpc, with most recent estimates converging toward $d \approx 3$ kpc (see Hayato et al. 2010, Figure 6), but its true value remains still rather uncertain. The derived ^{44}Ti mass as a function of the distance d is shown in Fig. 4. The red hatched area shows the region allowed by the BAT measurements. The blue hatched area includes the constraints from INTEGRAL (Renaud et al. 2006b).

The double degenerate scenario, which invokes the dynamical merger of two WDs, can produce ^{44}Ti masses between 2×10^{-4} and $5 \times 10^{-4} M_{\odot}$, consistent with our values. This scenario would be disfavored by the presence of a donor star for SN 1572 (Ruiz-Lapuente et al. 2004), which, however, was recently questioned by Kerzendorf et al. (2013).

In Figure 4 we also report the predicted isotope masses for different types of explosion models in the single degenerate scenario. Over the range of allowed distances, our results are broadly consistent with a sub-Chandrasekhar explosion producing a ^{44}Ti yield between 10^{-4} and $10^{-3} M_{\odot}$. Extreme models, such as the double detonation (models 1-4; Fink et al. 2010) or the helium deflagration scenarios (Woosley & Kasen 2011), are disfavored by the data.

Typical Ia explosions, such as the fast deflagration W7 (Nomoto et al. 1984) or centrally-ignited pure deflagrations (Travaglio et al. 2004), predict masses $< 10^{-5} M_{\odot}$, much lower than our inferred value. For $d \lesssim 3.5$ kpc, the BAT detection is consistent with some delayed detonation explosions. In particular, the WDD2, WDD3, and CDD2 models of Iwamoto et al. (1999), which also predict the largest amount of ^{56}Ni mass ($\sim 0.7 M_{\odot}$), and

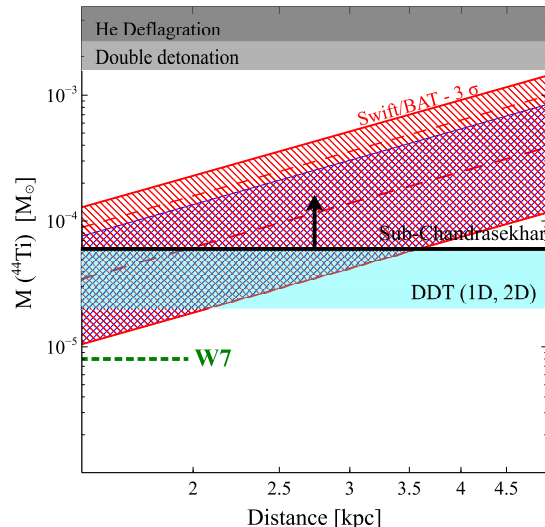


FIG. 4.— Mass of the radio-isotope ^{44}Ti , derived from the estimated line flux, as a function of the SNR distance. The red hatched area shows the 1σ (dashed line), and 3σ (solid line) confidence intervals from the *Swift*/BAT observations. The blue hatched area includes the 3σ upper limit from INTEGRAL observations. The mass range predicted by different explosion models is also reported.

the extremely off-center model O-DDT of Maeda et al. (2010). More recent three-dimensional simulations (Seitenzahl et al. 2013) predicts lower nucleosynthetic yields, marginally consistent with the derived range for $d \lesssim 2$ kpc. A delayed detonation explosion appears also consistent with the properties of the thermal X-ray emission (Badenes et al. 2006), and the SN 1572 light echo spectroscopy (Krause et al. 2008a).

4. SUMMARY AND CONCLUSION

The discovery of gamma-ray line emission at 1.157 MeV from the ^{44}Ti - ^{44}Sc - ^{44}Ca decay chain in Cas A (Iyudin et al. 1994) was a benchmark observation for the field of astronomy with radioactivities (see Diehl et al. 2007, for a recent review), as it established the production and ejection of ^{44}Ti from core collapse supernovae (ccSNe). The only other evidence for ^{44}Ti production came from the late time light curve of SN 1987A in the LMC, where modeling of the various contributions to power from radioactive decays indicated a ^{44}Ti mass of $0.2\text{--}2.0 \times 10^{-4} M_{\odot}$ (e.g. Fransson & Kozma 2002). The recent analysis of INTEGRAL observations of SN 1987A (Grebenev et al. 2012) confirmed the optical/NIR lightcurve estimates, but supporting values for the Ti yield at the upper end of their range.

With a galaxy wide star formation rate of order $3 M_{\odot}$ per year (see Diehl et al. 2006 for a review and a discussion of the use of another radioactive tracer, ^{26}Al , for measuring this rate) and a corresponding (IMF dependent) rate of 2-3 ccSNe per century one would expect several ^{44}Ti hot spots produced during a few mean lives of this isotope. Monte Carlo simulations of the distribution of supernovae in the Milky Way (The et al. 2006) indicated that the absence of additional ^{44}Ti sources is indeed statistically unlikely. The et al. (2006) concluded that either the Milky Way has experienced an unusually low core-collapse SN rate in the past few centuries, or that ^{44}Ti producing supernovae are rare, atypical events.

The BAT detection of ^{44}Ti in Tycho's supernova (Type Ia) would represent the third astrophysical site for which ^{44}Ti synthesis (and ejection into the ISM) has been established, indicating that both core collapse supernovae and thermonuclear (single degenerate) supernovae contribute to the galactic chemical evolution of ^{44}Ca . We now have two identified ^{44}Ti sources in the galaxy (a ccSN remnant, Cas A, and a Type Ia remnant, Tycho)

and one ccSN source in the LMC (SN 1987A), but this has not resolved the open question of the main source of ^{44}Ca in galactic chemical evolution. The yields of the three sources discussed here are surprisingly similar, higher than the predictions of standard SN models, and at a level that led to the expected multi-spot sky simulated by The et al. (2006). We are therefore still missing the key to understanding the origin of ^{44}Ca .

REFERENCES

- Ahmad, I., Greene, J. P., Moore, E. F., Ghelberg, S., Ofan, A., Paul, M., & Kutschera, W. 2006, *Phys. Rev. C*, 74, 065803
- Baade, W. 1945, *ApJ*, 102, 309
- Badenes, C., Borkowski, K. J., Hughes, J. P., Hwang, U., & Bravo, E. 2006, *ApJ*, 645, 1373
- Barthelmy, S. D., et al. 2005, *Space Sci. Rev.*, 120, 143
- Baumgartner, W. H., Tueller, J., Markwardt, C. B., Skinner, G. K., Barthelmy, S., Mushotzky, R. F., Evans, P. A., & Gehrels, N. 2013, *ApJS*, 207, 19
- Chieffi, A. & Limongi, M. 2013, *ApJ*, 764, 21
- Clayton, D. D., Colgate, S. A., & Fishman, G. J. 1969, *ApJ*, 155, 75
- Cusumano, G., et al. 2010, *A&A*, 510, A48
- Diehl, R., et al. 2006, *Nature*, 439, 45
- Diehl, R., Hartmann, D. H., & Prantzos, N. 2007, *Meteoritics and Planetary Science*, 42, 1145
- Dupraz, C., Bloemen, H., Bennett, K., Diehl, R., Hermsen, W., Iyudin, A. F., Ryan, J., & Schoenfelder, V. 1997, *A&A*, 324, 683
- Eriksen, K. A., et al. 2011, *ApJ*, 728, L28
- Fink, M., Röpke, F. K., Hillebrandt, W., Seitenzahl, I. R., Sim, S. A., & Kromer, M. 2010, *A&A*, 514, A53
- Fransson, C. & Kozma, C. 2002, *NewAR*, 46, 487
- Gehrels, N., et al. 2004, *ApJ*, 611, 1005
- Grebenev, S. A., Lutovinov, A. A., Tsygankov, S. S., & Winkler, C. 2012, *Nature*, 490, 373
- Grefenstette, B. W., et al. 2014, *Nature*, 506, 339
- Harrison, F. A., et al. 2013, *ApJ*, 770, 103
- Hayato, A., et al. 2010, *ApJ*, 725, 894
- Hwang, U., Decourchelle, A., Holt, S. S., & Petre, R. 2002, *ApJ*, 581, 1101
- Iwamoto, K., Brachwitz, F., Nomoto, K., Kishimoto, N., Umeda, H., Hix, W. R., & Thielemann, F.-K. 1999, *ApJS*, 125, 439
- Iyudin, A. F., et al. 1994, *A&A*, 284, L1
- Kerzendorf, W. E., et al. 2013, *ApJ*, 774, 99
- Kothes, R., Fedotov, K., Foster, T. J., & Uyaniker, B. 2006, *A&A*, 457, 1081
- Krause, O., Birkmann, S. M., Usuda, T., Hattori, T., Goto, M., Rieke, G. H., & Misselt, K. A. 2008a, *Science*, 320, 1195
- Krause, O., Tanaka, M., Usuda, T., Hattori, T., Goto, M., Birkmann, S., & Nomoto, K. 2008b, *Nature*, 456, 617
- Lampton, M., Margon, B., & Bowyer, S. 1976, *ApJ*, 208, 177
- Leising, M. D. 2001, *ApJ*, 563, 185
- Maeda, K., Röpke, F. K., Fink, M., Hillebrandt, W., Travaglio, C., & Thielemann, F.-K. 2010, *ApJ*, 712, 624
- Nomoto, K., Thielemann, F.-K., & Yokoi, K. 1984, *ApJ*, 286, 644
- Renaud, M., et al. 2006a, *ApJ*, 647, L41
- Renaud, M., Vink, J., Decourchelle, A., Lebrun, F., Terrier, R., & Ballet, J. 2006b, *NewAR*, 50, 540
- Reynolds, S. P. & Keohane, J. W. 1999, *ApJ*, 525, 368
- Ruiz-Lapuente, P., et al. 2004, *Nature*, 431, 1069
- Segreto, A., Cusumano, G., Ferrigno, C., La Parola, V., Mangano, V., Mineo, T., & Romano, P. 2010, *A&A*, 510, A47
- Seitenzahl, I. R., et al. 2013, *MNRAS*, 429, 1156
- Slane, P., Lee, S.-H., Ellison, D. C., Patnaude, D. J., Hughes, J. P., Eriksen, K. A., Castro, D., & Nagataki, S. 2014, *ApJ*, 783, 33
- Tamagawa, T., et al. 2009, *PASJ*, 61, 167
- The, L.-S., et al. 2006, *A&A*, 450, 1037
- Travaglio, C., Hillebrandt, W., Reinecke, M., & Thielemann, F.-K. 2004, *A&A*, 425, 1029
- Tueller, J., et al. 2010, *ApJS*, 186, 378
- Vink, J. 2012, *A&A Rev.*, 20, 49
- Vink, J., Laming, J. M., Kaastra, J. S., Bleeker, J. A. M., Bloemen, H., & Oberlack, U. 2001, *ApJ*, 560, L79
- Wang, W. & Li, Z. 2014, *ApJ*, 789, 123
- Woosley, S. E. & Kasen, D. 2011, *ApJ*, 734, 38
- Woosley, S. E. & Weaver, T. A. 1994, *ApJ*, 423, 371